ACS Sustainable Chemistry & Engineering

pubs.acs.org/journal/ascecg

Research Article

SERS Enhancement of Porphyrin-Type Molecules on Metal-Free Cellulose-Based Substrates

Agata Fularz, Sawsan Almohammed, and James H. Rice*

Cite This: *ACS Sustainable Chem. Eng.* 2021, 9, 16808–16819

Read Online

ACCESS | Metrics & More | Article Recommendations | Supporting Information

ABSTRACT: The detection of analytes using spectroscopy methods, such as surface-enhanced Raman spectroscopy (SERS), is crucial in the fields of medical diagnostics, forensics, security, and environmental monitoring. In recent years, a lot of focus has been directed toward organic polymer material-based SERS platforms due to their lower cost, controllable synthesis and fabrication, structural versatility, as well as biocompatibility and biodegradability. Here, we report that cellulose nanofiber-based substrates can be used as a metal-free SERS platform for the detection of porphyrin-type molecules. We report SERS signal enhancement for five different porphyrin molecules with exceptional 2 orders of magnitude peak intensity enhancement observed resulting in a detection limit of 10^{-5} M. We show that the cellulose-based platform is more suitable for porphyrin molecule detection than traditionally used semiconductor materials like graphene oxide. The observed enhancement is attributed to the disturbed growth of self-assembled structures on the cellulose nanofibers and the generation of disordered 3D clusters of porphyrin molecules.

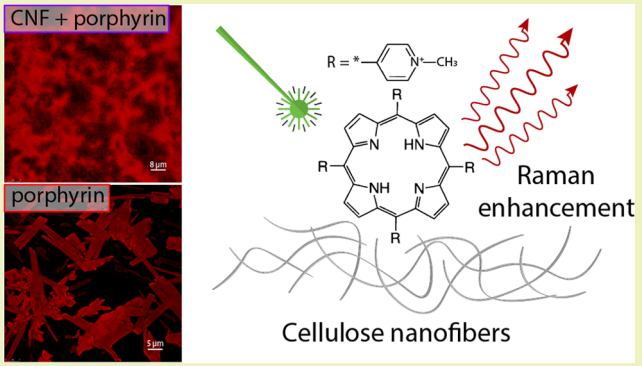

KEYWORDS: *cellulose, cellulose nanofibers, polymers, surface-enhanced Raman spectroscopy, SERS, Raman*

INTRODUCTION

Surface-enhanced Raman spectroscopy (SERS) is a sensitive analytical technique used for the detection of chemical and biological molecules by irradiating them with laser light, which allows for the identification of specific vibrational modes of the chemical components.[1] The Raman signal intensity of molecules deposited on SERS-active substrates is significantly enhanced, enabling precise molecular identification, making the technique widely applicable in the fields of medical diagnostics, forensics, security, and environmental monitoring.[2−6] The primary contribution to the SERS performance of a given substrate is the electromagnetic enhancement arising from the excitation of a localized surface plasmon resonance (LSPR) in a metal particle with a size comparable to the wavelength of the incident light.[7,8] Chemical enhancement is a secondary weaker process resulting in enhancement of the signal by up to 2 orders of magnitude and is usually assigned to the process of charge being transferred between the substrate and the analyte molecule.[9] Although metal-based SERS substrates are more efficient (enhancement factor ~10^6), recently researchers focused on alternative substrate designs based on semiconductor materials to circumvent limitations of metal-based SERS platforms, such as lack of biocompatibility and inertness, as well as the high cost of materials and manufacturing.[10]

The use of organic materials with a focus on polymers as a SERS platform has been explored in recent years due to their lower cost, controllable synthesis and fabrication, and structural versatility.[11] Cellulose is an abundant, biodegradable, and sustainable organic polymer that is present in plants, bacteria, fungi, and algae that consists of many D-glucose units linked by glycosidic bonds.[12] Cellulose nanofibers (CNF) are a type of nanostructured cellulose arranged into one-dimensional structures with length in the micrometer range and diameter up to several hundred nanometers.[13] The nanofibers consist of connected crystalline and amorphous regions of cellulose and have been investigated for potential applications in material science, in particular for device manufacturing[14] and as biodegradable plastic alternatives.[15,16]

Cellulose-based materials have been previously explored as platforms for surface-enhanced Raman spectroscopy due to their biocompatibility, roughness, large surface area,[17] flexibility, and ability to be functionalized[18] or loaded with nanoparticles.[13] Cellulose-based materials combined with

Received: September 30, 2021
Revised: November 24, 2021
Published: December 2, 2021

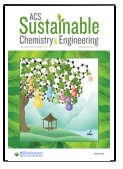

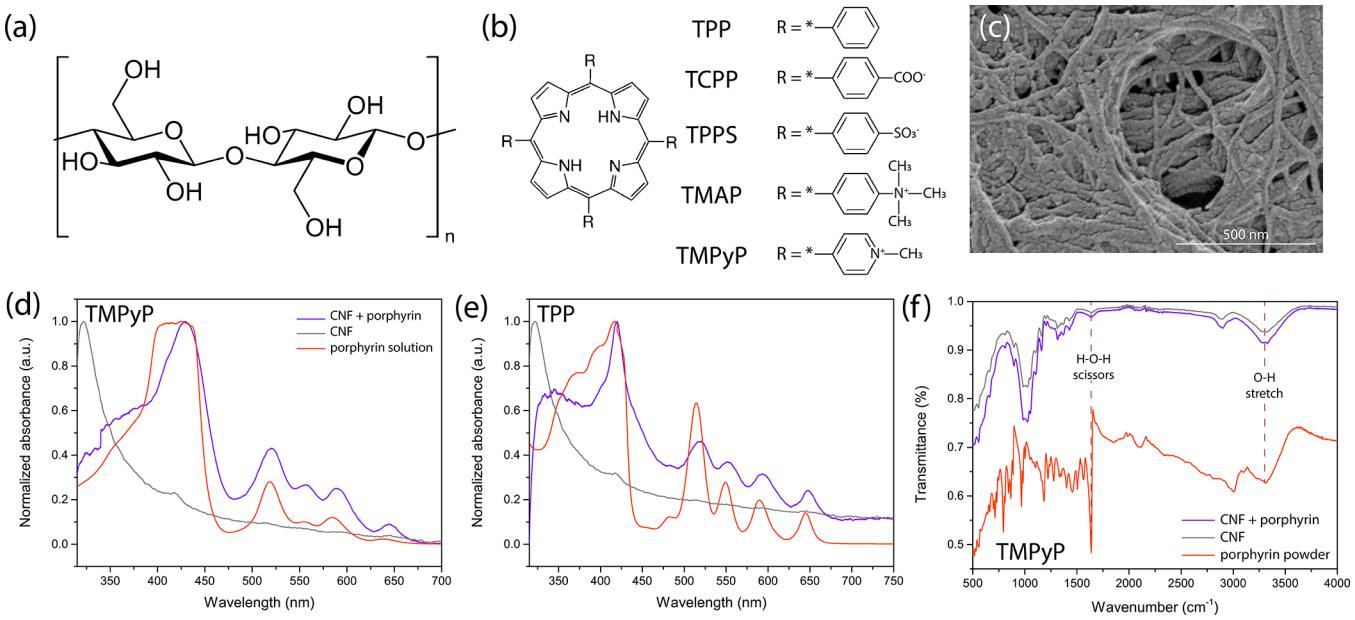

Figure 1. (a) Chemical structure of a cellulose molecule and (b) the porphyrin molecules used in the experiment. (c) SEM image of cellulose nanofibers on a silicon substrate. Normalized UV−vis absorption spectra of (d) TMPyP and (e) TPP porphyrin at 10^{-3} M concentration deposited on CNF compared to the background spectrum of CNF and the spectrum of the porphyrin in solution. (f) FTIR spectra of CNF compared to the spectrum of a sample porphyrin molecule (10^{-4} M TMPyP) on CNF and in powder form.

either gold[13,19] or silver[17,20,21] as well as photonic and plasmonic crystals based on cellulose-derivative-based materials[16,22,23] have been shown to be efficient at Raman signal enhancement. CNF/metal composites are effective at detecting a wide variety of analyte molecules including pesticides and other important biological species down to the sub-attomolar level.[20] The studies on cellulose have however focused on combining the polymer with noble metals, limiting the applicability of the platform for the detection of biological molecules.

In this study, we show that metal-free cellulose nanofiber (CNF) platforms can be employed as SERS substrates for the detection of porphyrin-type molecules. Porphyrins are a group of organic tetrapyrrole compounds of great biological importance.[24] Porphyrins and their naturally occurring derivatives (metal complexes), as well as other related species, play an important role in the transport and storage of oxygen,[25,26] driving oxidation reactions in organic compounds,[24,27] and in the process of photosynthesis.[28−30]

We report SERS signal enhancement for five different porphyrin molecules with exceptional 2 orders of magnitude peak intensity enhancement observed for meso-tetra(*N*-methyl-4-pyridyl)porphine tetrachloride (TMPyP). We show that TMPyP can be detected on CNF at concentrations as low as 10^{-5} M, making the platform a more suitable metal-free SERS substrate for porphyrin molecules than traditionally used organic semiconductor materials like graphene oxide.

RESULTS AND DISCUSSION

The chemical structures of a cellulose molecule and the porphyrin-type molecules used as analytes are shown in Figure 1a,b, respectively. In the study, we used a wide variety of porphyrins, including neutral hydrophobic tetraphenyl porphyrin (TPP), as well as water-soluble molecules: two cationic species (TMPyP neutralized by Cl^- ions and TMAP with *p*-toluenesulfonic acid used as counterion) and two anionic species (TPPS neutralized by Na^+ and TCPP neutralized by H^+).[31,32] The cellulose nanofiber (CNF) platform was prepared by drop-casting a nanofiber dispersion on a silicon piece and drying out the solvent. Figure 1c shows a scanning electron microscopy (SEM) image of the substrate fabricated using a highly concentrated (1 wt %) cellulose dispersion showing a thick layer of randomly distributed nanofibers. The length of the fibers was in the micrometer range while their width was determined to be 88 ± 37 nm, suggesting that the fibers could consist of bundles of several smaller elementary fibrils with a diameter of about 3 nm.[33]

Figure 1d,e shows the normalized UV−vis spectra of the porphyrin solution, the CNF substrate, and the porphyrin on CNF for TMPyP and TPP, respectively. Cellulose absorbs UV light as shown in the UV−vis spectrum consisting of a broad peak centered around 322 nm, in agreement with data previously reported in the literature.[34,35] Both TMPyP and TPP are characterized by a broad, high-intensity Soret band and four lower-intensity Q bands in the UV−vis spectrum.[36] Upon addition of the porphyrins to the CNF substrate, the peak associated with cellulose becomes less prominent and the Q and Soret become slightly red-shifted, suggesting possible *J*-aggregation of the molecules on the cellulose substrate.[37,38] Figure 1f shows the FTIR spectra of TMPyP in powder form and on CNF compared to the CNF substrate only. The spectrum of TMPyP is characterized by peaks at 713 cm^{-1} (N−H bending), 793 cm^{-1} (C−H bending), 1456 and 1402 cm^{-1} (C−N stretching and bending), 1559 cm^{-1} (C═C stretching), as well as 1637 cm^{-1} (C═N stretch vibration of pyridyl rings).[39,40] Upon the addition of the porphyrin solution on cellulose nanofibers, peaks associated with the porphyrin could not be distinguished in the spectrum. The FTIR peaks associated with cellulose are peaks in the 1030 and 1314−1372 cm^{-1} range that can be assigned to C−H bending vibrations.[34,35] Additionally, the bands at 1059−1162 cm^{-1} correspond to C−O and C−O−C stretching,[34] while a small

https://doi.org/10.1021/acssuschemeng.1c06685
ACS Sustainable Chem. Eng. 2021, 9, 16808−16819

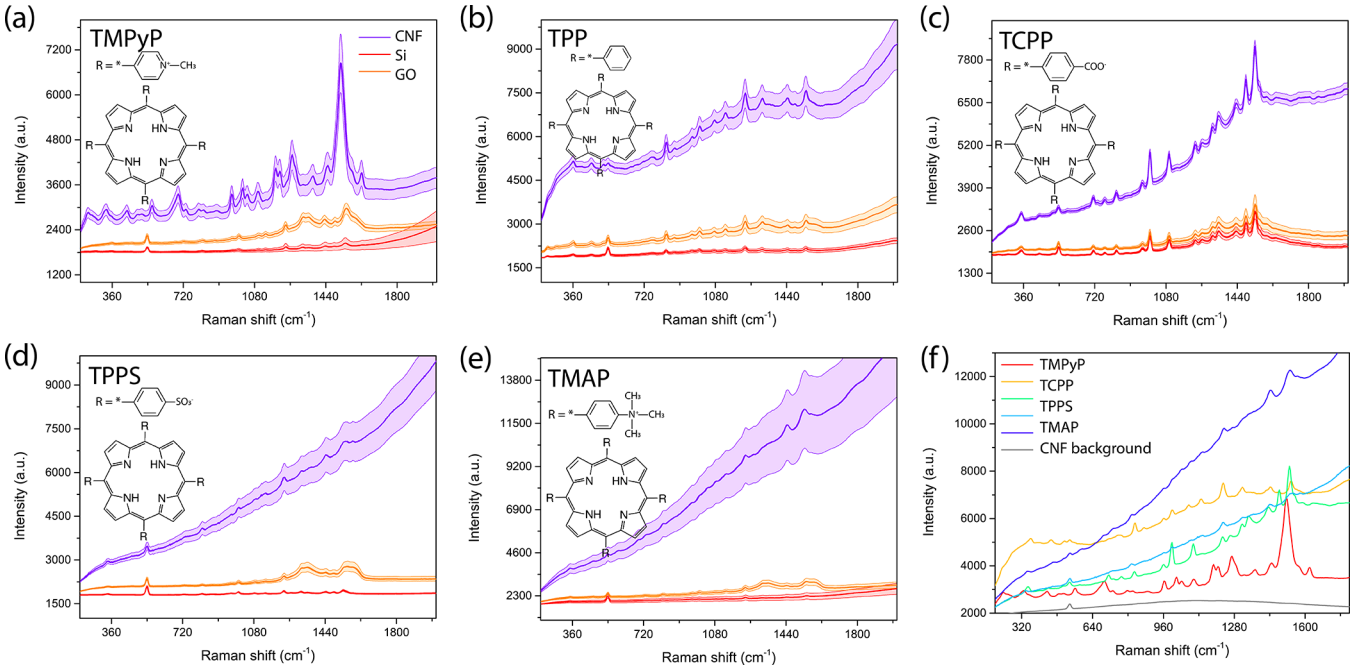

Figure 2. SERS spectra of the porphyrin molecules on CNF compared to the spectra on graphene oxide and silicon for 10^{-3} M (a) TMPyP, (b) TPP, (c) TCPP, (d) TPPS, and (e) TMAP. (f) Spectra for all of the porphyrin molecules used on CNF compared to the Raman background signal of cellulose.

Table 1. Raman Enhancement Obtained for Porphyrin Molecules Used Deposited on CNF Compared to the Silicon Substrate

Analyte molecule	Ligand	Counterion	Raman enhancement I_{CNF}/I_{Si}	Relative Raman enhancement $(I_{CNF}-I_{CNF\text{-}background})/(I_{Si}-I_{Si\text{-}background})$
TPP	R = *	-	3.4	7.0
TMPyP	R = * N^+—CH_3	Cl^-	2.5	96.0
TMAP	R = * CH_3, N^+, CH_3, CH_3	H_3C, SO_3^-	5.4	16.2
TPPS	R = * SO_3^-	Na^+	3.6	6.4
TCPP	R = * COO^-	H^+	2.6	2.1

peak at 897 cm^{-1} is associated with β-glycosidic linkages in the cellulose structure.[41] Peaks associated with Iα and Iβ cellulose allomorphs at 750 and 710 cm^{-1} could not be distinguished, suggesting that amorphous cellulose predominates over crystalline cellulose in the sample.[42] Two broad bands observed at 1635 and 3300 cm^{-1} are associated with H−O−H scissors and O−H stretching. The peaks are reduced in intensity upon drying of the sample, which suggests they are mostly associated with the presence of water molecules in the sample.[43]

Following characterization, the CNF substrates were employed as metal-free SERS platforms for the detection of porphyrin molecules. Figure 2a−e shows the SERS spectra of the five different porphyrin molecules on CNF, graphene oxide (GO), and silicon, while Figure 2f shows all of the spectra compared to the background signal of CNF. Silicon is a semiconductor material often used as a control substrate for SERS measurements due to its Raman spectrum consisting of one peak at 520 cm^{-1}, limiting the background signal associated with the substrate.[44] Graphene-based platforms

https://doi.org/10.1021/acssuschemeng.1c06685
ACS Sustainable Chem. Eng. 2021, 9, 16808−16819

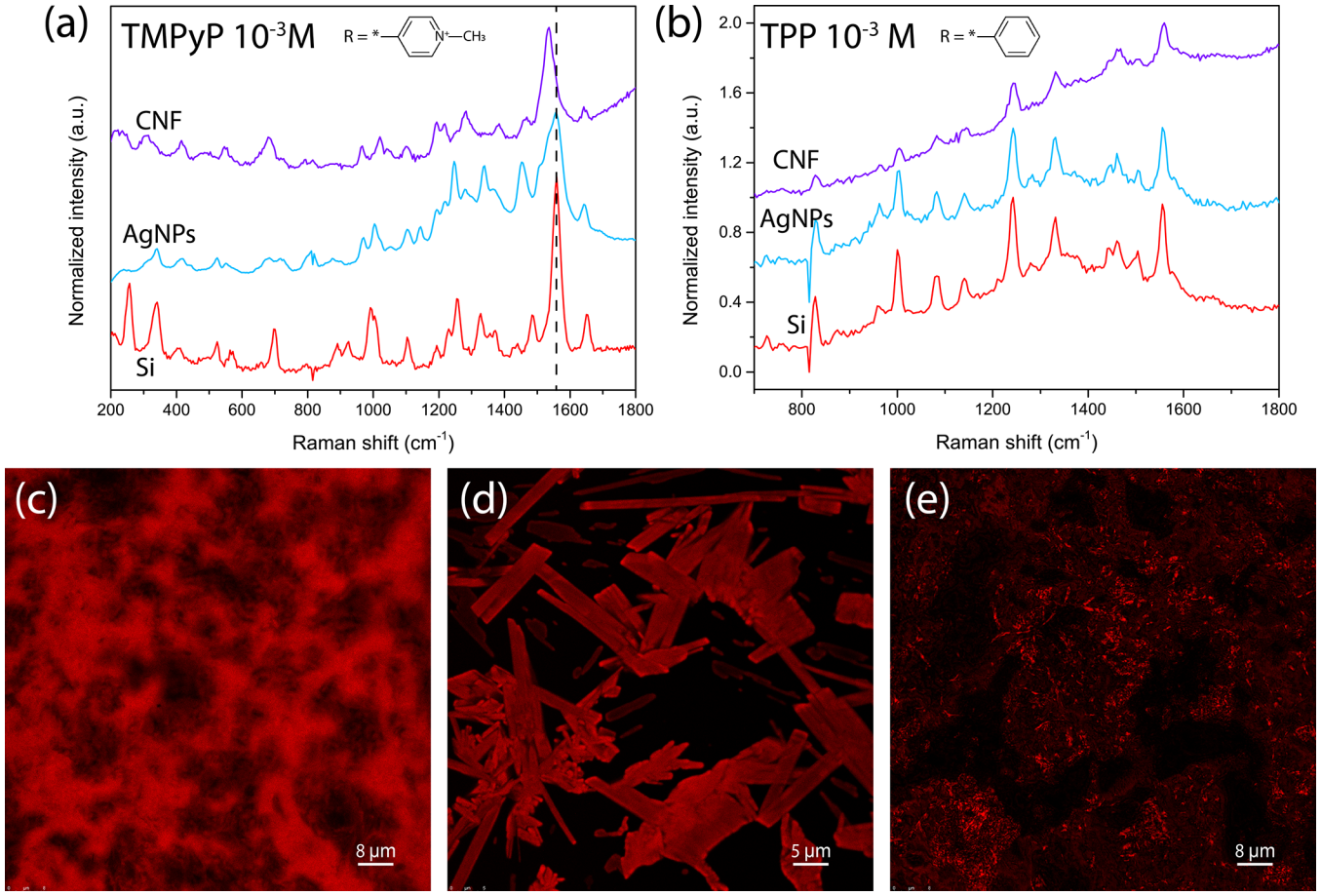

Figure 3. Normalized SERS spectra of 10^{-3} M (a) TMPyP and (b) TPP on CNF, AgNPs, and Si showing the shift in the position of the peaks. Fluorescence confocal microscopy images of (c) TMPyP on CNF, (d) TMPyP, and (e) CNF only showing the difference in the porphyrin structure.

such as graphene oxide are a class of SERS-active metal-free materials that have been recently explored due to their unique two-dimensional structure as well as physical and chemical properties, such as stability and biocompatibility.[45−47] The graphene-enhanced Raman spectroscopy (GERS) effect is considered to be absent from electromagnetic enhancement, making it a pure system for the investigation of the chemical enhancement process.[48,49] Here, randomly distributed graphene oxide was used to assess the efficiency of the CNF substrate and compare it to a different plasmon-free SERS-active platform.

The peaks in the SERS spectrum of TMPyP deposited on silicon can be assigned to C-pyrrole bending (1254 cm^{-1}), C−N stretching (1327 cm^{-1}), C−C stretching (1484 and 1559 cm^{-1}), and in-plane phenyl ring bending (1625 cm^{-1}), in agreement with values previously reported in the literature.[50−52] TPP, the simplest of the porphyrins used in the experiment, has a spectrum with characteristic peaks at 834, 1231, and 1538 cm^{-1} assigned to phenyl ring bending, C-phenyl stretching, and C−C stretching, respectively.[53,54] TCPP has characteristic peaks at 1000 (phenyl ring deformation), 1096 (pyrrole in-plane bending), 1345 and 1530 (phenyl in-plane bending), as well as 1484 cm^{-1} (C−C stretching).[55] TPPS is characterized by a spectrum similar to that of TPP: phenyl ring bending peak at 818 cm^{-1}, C-phenyl stretching at 1231 cm^{-1}, and several peaks associated with C−C stretching (1442, 1484, 1530 cm^{-1}).[51,54] The spectrum of TMAP differs only slightly from that of TMPyP; strong intensity peaks are observed at 1235 (C-pyrrole bending), 1442, and 1542 cm^{-1} (C−C stretching).[51,52] A more detailed assignment of the bands of the porphyrin-like molecules can be found in the references provided.

Five different porphyrin molecules were investigated as analyte molecules for SERS; four of them (TMPyP, TCPP, TPPS, and TMAP) are water-soluble porphyrins, characterized by solubility in aqueous solutions at pH ≥7 and concentrations >1 mM at room temperature.[56] TPP is not water-soluble and was dissolved in dichloromethane. Following the deposition of the porphyrins on the CNF substrate, we observed an enhancement in the Raman spectrum for all of the analyte molecules used. Both the overall and the relative background-subtracted relative intensity of the peaks were determined, as outlined in Figure S1 in the Supporting Information. The relative enhancement of the Raman peaks varied from 2.1-fold for TCPP up to 96-fold for TMPyP compared to the analytes deposited directly on silicon. The summary of the observed enhancements is shown in Table 1. Although the Raman signal also increased for GO substrates, the enhancement was lower than 2-fold for the randomly distributed nanoplatelets. Additionally, the Raman spectrum of graphene is characterized by two broad Raman peaks at 1350 cm^{-1} (D band) and 1580 cm^{-1} (G band), which may obstruct the peaks associated with the presence of analytes, reducing the applicability of graphene-based metal-free platforms.[57] Cellulose nanofibers

https://doi.org/10.1021/acssuschemeng.1c06685
ACS Sustainable Chem. Eng. 2021, 9, 16808−16819

although characterized by low-intensity fluorescence background have not been shown to have Raman peaks in the 200−2000 cm^{-1} range, as shown in Figure 2f, making them more applicable to detect porphyrins. The intensity of the Raman signal of the porphyrin molecules did not vary significantly when a coverslip, a different inert supporting substrate, was used underneath the cellulose nanofibers. For TMPyP on CNF, a variation of 30% in the signal strength was observed, which can be attributed to surface roughness and small variations in the wettability of the coverslip and silicon, resulting in a differing thickness of the deposited cellulose layer. When TMPyP was deposited directly on silicon or coverslip, a variation of 7% in signal intensity was observed (Figure S2). The reproducibility of the Raman signal obtained from the CNF substrates with TMPyP used as an analyte was also studied, as outlined in Figure S3. Ideally, for a SERS substrate, a low variation in the strength of generated signal obtained from different spots on the sample is desirable. Although the CNF substrate is characterized by relatively high roughness, which may lower the reproducibility of the SERS signal, a 14.6% relative standard deviation in the signal intensity was observed, reaching the 15% threshold value desired for quantitative Raman studies.[44] Nonporphyrin molecules often used for assessing the performance of Raman substrates were also used (Figure S4) with up to 2-fold overall enhancement measured. Since the highest enhancement reaching almost 2 orders of magnitude in relative peak intensity has been observed for TMPyP, further analysis has focused on the porphyrin molecules.

Figure 3a shows the normalized spectra of TMPyP on silicon and cellulose nanofibers compared to traditionally used in SERS metal-based substrate consisting of randomly distributed silver nanoparticles (AgNPs) on silicon. The peak positions in the Raman spectrum of TMPyP change significantly upon adsorption on cellulose, for instance, the position of the highest intensity peak at 1559 cm^{-1} and C−C stretching becomes shifted down to 1535 cm^{-1}, which is a value within the range associated with C−C stretching for the other porphyrins. The spectrum of TPP on the different substrates does not change, as outlined in Figure 3b.

Porphyrins are known to self-assemble into nanostructures such as nanorods, nanotubes, and nanosheets, depending on the synthesis method.[58] Depending on the environment, porphyrins can crystallize into different forms; for instance, both triclinic and tetragonal crystal systems have been observed and analyzed for TPP, one of the simplest porphyrin-type molecules.[59,60] In our study, relatively large numbers of porphyrin molecules were deposited on the supporting Si, GO, and CNF substrates (above 100 monolayers as outlined in Table S1), which would allow for an assembly of a porphyrin crystal.

The different vibrational properties of TMPyP on CNF and Si could be explained by the generation of different crystalline or crystalline and amorphous porphyrin adlayers. Figure 3c−e shows fluorescence confocal microscopy images of TMPyP on CNF and deposited directly on a coverslip compared to an image of cellulose nanofibers with no dye on them. On cellulose, the porphyrin seems to be distributed uniformly all over the sample and no distinguishable porphyrin nanostructures can be observed. For the control sample, however, the sample consists of nanorods with lengths in the range of 3−30 μm and an average width of 1.6 ± 0.9 μm. The distribution of the dye in the porphyrin on the CNF sample resembles that of the low-intensity autofluorescence signal obtained from the cellulose nanofibers, suggesting that the dye molecules adsorb to the cellulose, despite the large adsorption energy of around 400 kJ/mol per molecule for TMPyP on different cellulose surfaces at room temperature.[61]

We have previously published a detailed analysis of the morphology of porphyrin-type adlayer on cellulose substrates using molecular dynamics simulations based on atomistic empirical force fields.[61] The data have shown that both TPP and TMPyP assemble in an ordered manner with the molecule lying flat on the cellulose surface when the coverage is limited to less than one monolayer. The growth however changes to irregular 3D cluster formation at coverage exceeding 60% of monolayer formation, due to low mobility of the TPP and TMPyP molecules. Similar experimental studies were previously performed for porphyrin-like molecules on organic substrates, showing a similar tendency toward epitaxial growth of TPP and generation of 3D clusters.[62−64] The adlayer, therefore, is most likely to be amorphous, with the possibility of the growth of crystallites with a prevalent molecular orientation.

We can infer that the presence of cellulose disrupts the nanorod assembly process of TMPyP, resulting in a change of the structure of the adlayer from ordered to disordered and a shift in the peak position in the Raman spectrum. The disordered growth of the TMPyP molecules on the CNF substrate and the generation of 3D clusters could also explain the increased Raman signal intensity. Aggregation of the porphyrin in certain spots of the sample would artificially increase the concentration of the molecules, making them easier to detect via Raman spectroscopy. Figures S7 and S8 show additional SEM and confocal images of TPP and TMPyP on the different substrates used in this study (CNF, AgNPs, GO, Si). The images confirm that while the structure of TMPyP varies on CNF when compared to the other samples, TPP forms similar structures on CNF and when cellulose is not present, resulting in a similar distribution of molecules for both the control and the cellulose samples.

Additionally, we have determined that the electrostatic interactions between the porphyrin adlayer and the cellulose surface could affect the vibrational properties of the samples.[61] The Cl^- counterion of TMPyP is attracted to the positively charged end (proton) of the −OH groups in the cellulose structure, resulting in the generation of a nonvanishing dipole moment in the porphyrin adlayer. The average dipole moment per unit surface area was shown to increase with the growth of the number of adsorbed porphyrin molecules, reaching values of 1−1.7 Debye/nm^2 for three monolayers of TMPyP on different cellulose surfaces. Due to the interaction with cellulose, the two surfaces of the porphyrin adlayer (that is the interface between the cellulose and the porphyrin as well as the free porphyrin surface in contact with air) become charged, resulting in the generation of an electric field in the porphyrin layer, which could both enhance the intensity and shift the position of Raman peaks in the spectrum. The suggested mechanism could explain the observed differences in the enhancements for the different porphyrin molecules, as the neutral and anionic porphyrins could not interact with the −OH groups of the cellulose in a similar fashion. TMAP, the second cationic porphyrin we used in the study was also characterized by high Raman signal enhancement on cellulose surfaces, although about 5 times smaller than that of TMPyP. This suggests that not only the charge but also the size of the

https://doi.org/10.1021/acssuschemeng.1c06685
ACS Sustainable Chem. Eng. 2021, 9, 16808−16819

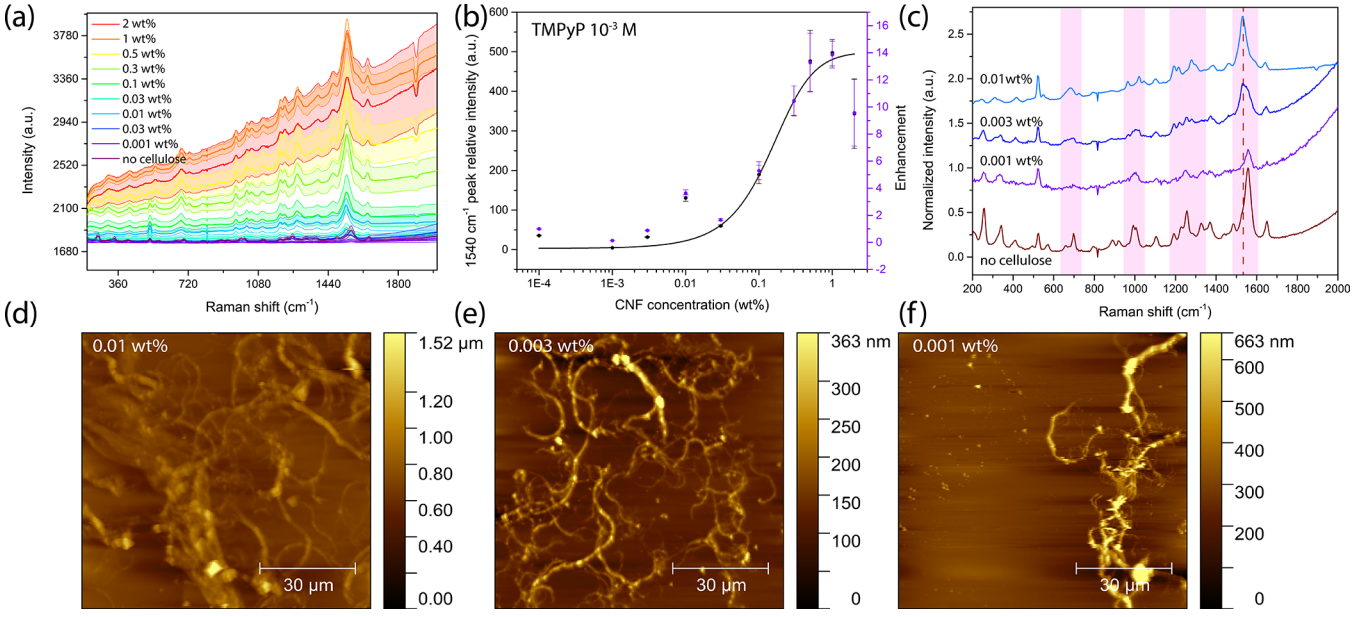

Figure 4. (a) Raman spectra of 10^{-3} M TMPyP deposited on a CNF substrate following dilution of the CNF dispersion to various concentrations prior to being drop-cast and (b) the dependence of the 1540 cm^{-1} peak intensity (black) and the SERS enhancement compared to Si-only substrate (purple) on the CNF dispersion concentration. (c) Raman spectra of TMPyP on highly diluted CNF, showing the shift in the spectrum. (d–f) AFM images of diluted CNF on silicon for 0.01, 0.003, and 0.001 wt % CNF, respectively.

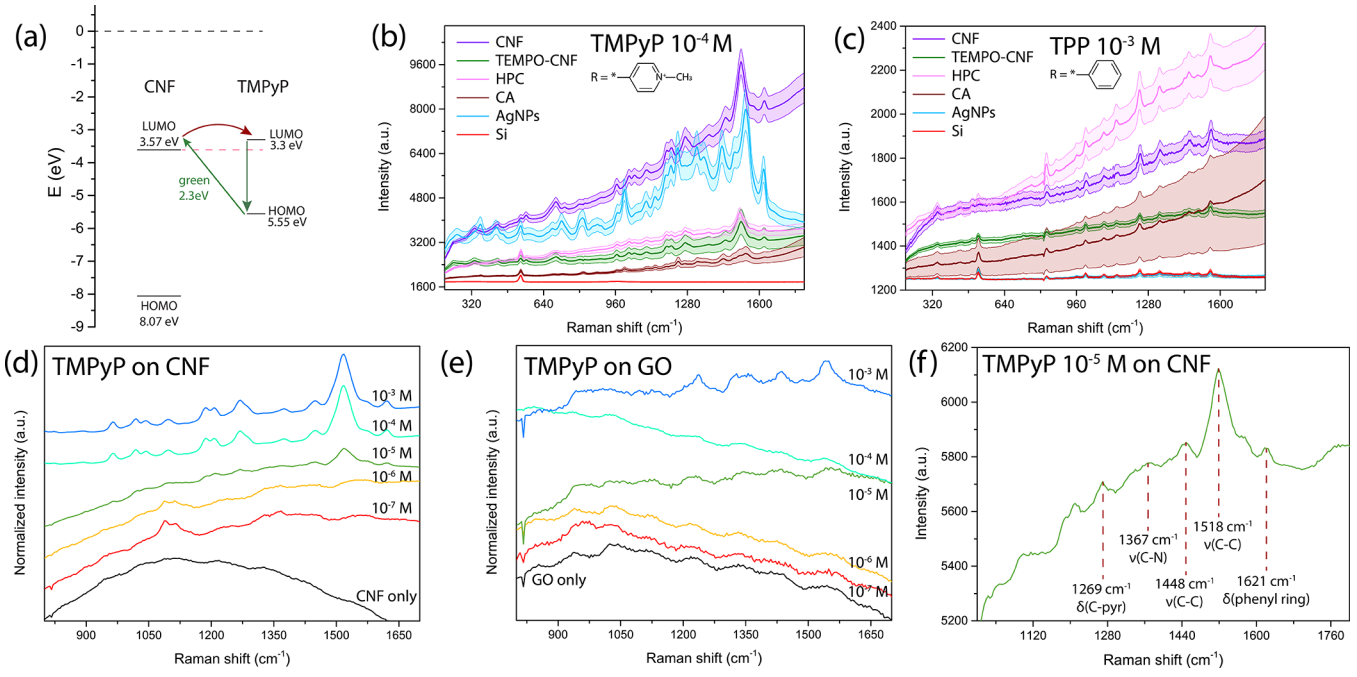

Figure 5. (a) Proposed band diagram showing a possible charge transfer between the CNF substrate and a TMPyP molecule. SERS spectra of porphyrins on different types of cellulose-based substrates compared to silver nanoparticles and silicon for (b) 10^{-4} M TMPyP and (c) 10^{-3} M TPP. Normalized SERS spectra of TMPyP on (d) CNF and (e) GO used for the determination of the detection limit. (f) Spectrum of 10^{-5} M TMPyP on CNF, highlighting the low detection limit on the metal-free substrate.

ion affect the mechanism, as the *p*-toluenesulfonic acid (PTSA) used for neutralization of TMAP is much larger than the Cl^-, hampering the preferential adsorption on cellulose surfaces. To further investigate the effect the counterion in the porphyrin structure has on the SERS enhancement observed, we collected additional spectra of TMPyP with *p*-toluenesulfonic acid used for neutralization on both CNF and Si, as outlined in Figure S9. The relative SERS signal of TMPyP on CNF was 1.7 times higher for the molecule with a Cl^- ion. Additionally, the Raman signal of TMPyP with a Cl^- ion was lower in intensity when compared to PTSA, showing that the addition of cellulose has a more significant effect on the TMPyP/Cl^- molecule. The SERS signal was 19.3 times higher when the Cl^- counterion was used and only 5.9 times higher for PTSA, further proving that the structure of the porphyrin affects the SERS spectrum obtained.

https://doi.org/10.1021/acssuschemeng.1c06685
ACS Sustainable Chem. Eng. 2021, 9, 16808−16819

We analyzed the effect of reducing the concentration of CNF dispersion in water prior to its deposition on the silicon substrate. Figure 4a shows the SERS spectra of 10^{-3} M TMPyP deposited on 30 μL of dried CNF on Si at concentrations varying from 2 to 0.001 wt % compared to the spectrum of TMPyP on Si. The intensity of the Raman signal decreases steadily with the decrease in CNF concentration, resulting in the reduction of the coverage of the silicon substrate with cellulose nanofibers (Figure 4b). The previously described shift in the peak position in the spectrum can be observed when the CNF concentration is reduced from 0.003 to 0.001 wt %, as shown in Figure 4c. Figure 4d–f shows AFM images of the highly diluted cellulose, showing that at the point of transition only individual nanofibers are present in the sample. The data show that it is possible to distinguish between the spectrum of TMPyP on CNF and Si, and that TMPyP has an affinity to bind to the cellulose surface, even when not many fibers are present in the sample.

A charge transfer process driven by the green laser light could be a mechanism contributing to the observed SERS enhancement on CNF substrates. Figure 5a depicts a proposed band diagram showing a possible charge transfer between the CNF substrate and a TMPyP molecule, characterized by the highest observed enhancement. TMPyP has its highest occupied molecular orbital (HOMO) and lowest unoccupied molecular orbital (LUMO) levels positioned 5.55 and 3.3 eV below the vacuum level, respectively.[65] The optical band gap of nanofibrillated cellulose has been previously reported to be 4.5 eV with its highest occupied molecular orbital (HOMO) level being positioned 8.07 eV below the vacuum level.[15,66] The green laser light used for Raman measurements provides energy equal to 2.3 eV, which is not enough energy to drive the charge transfer process from the substrate to the analyte molecules. The charge however can be excited from the HOMO level of the molecule directly to the LUMO level of the cellulose. The charge could then be transferred back to the ground state of the porphyrin while leaving it at some vibrational state, resulting in an emission of a Raman photon. The energy required for such a process to take place is lower than the energy provided by the green laser and lower than the energy required to excite charge in TMPyP directly, meaning that the presence of cellulose in the sample may facilitate charge generation and therefore increase the intensity of the scattered light. The charge transfer mechanism described here would be similar for all of the porphyrin molecules studied due to the fact that they are characterized by similar HOMO and LUMO values, likely associated with the tetrapyrrole ring (Figure S10). This suggests that although a charge transfer can take place and contribute to the observed enhancement, other effects correlated with the porphyrin structure need to take place to explain the large variation in the enhancement factor values observed for the different molecules.

Cellulose is a versatile material that can be easily modified by partially replacing the hydroxyl (−OH) groups in the structure. In this study, we utilized different types of cellulose derivatives as SERS substrates for the detection of TMPyP and TPP, as shown in Figure 5b,c, to better understand the enhancement mechanism observed. TEMPO-oxidized cellulose nanofibers (TEMPO-CNF), cellulose acetate (CA), and hydroxypropyl cellulose (HPC) are characterized by the presence of carboxyl, acetyl, and $OCH_2CH(OH)CH_3$ groups in their structure, respectively. The detailed chemical structures of the different types of cellulose materials are outlined in Figure S11. The spectra of TPP on the different types of cellulose as well as Si and AgNPs are very similar with the best signal being observed on HPC and CNF. TMPyP, on the other hand, is easily identifiable on the different types of cellulose-based substrates, even when the concentration is reduced to 10^{-4} M, with the spectrum on CNF being comparable in intensity to that of TMPyP on AgNPs. The different cellulose substrates studied are characterized by different roughnesses and therefore varying surface areas, which may affect the molecule adsorption; we have however determined that the changes in the surface area for the different materials were insignificant when compared to the SERS signal enhancement observed with Si substrate used as a control (Figures S12, S13 and Table S2). Additionally, we studied the wettability of the different cellulose-based substrates (shown in Figure S14), as it may be a contributing factor to the observed SERS enhancement, especially for deposition of materials from aqueous solution. Higher hydrophilicity of the substrate results in the spreading of the molecule solution, which would increase the surface area for adsorption of the molecules to the cellulose surface. On the other hand, more hydrophobic surfaces have been shown to be beneficial for SERS, as they concentrate molecules in one spot of the sample, resulting in an artificial increase of the concentration, and therefore, the SERS signal intensity. Nonetheless, based on contact angle measurements of CNF, TEMPO-CNF, CA, and HPC, we have not observed a clear relationship between the wettability of the substrate and the SERS enhancement and thus we excluded wettability and roughness-related effects from further discussion of the enhancement mechanism. The similar performance of the different types of cellulose suggests that the interaction between the cellulose backbone and the tetrapyrrole ring of the porphyrin could affect the arrangement of molecules on the substrate and therefore contribute to the high Raman signal enhancement observed. Additionally, the data shows that replacing the −OH groups in the cellulose substrate results in a reduction of the Raman signal intensity, further confirming that the interaction between the TMPyP counterion and the substrate is a contributing factor. HPC and TEMPO-CNF are characterized by similar enhancement, while CA performed the worst out of all of the cellulose-based substrates, which could be related to the structure of functional groups in the materials. While both −COOH and $OCH_2CH(OH)CH_3$ contain −OH groups in their structure, cellulose acetate is modified with CH_3CO, which would result in a different charge distribution, and therefore affect the interaction of the substrate with porphyrins. Additionally, CA is characterized by a quite strong fluorescent background signal (as shown in Figure S13), which may mask some of the Raman peaks in the spectrum, reducing the efficiency of the material as a SERS substrate.

Subsequently, we determined the detection limit of TMPyP on the metal-free CNF and GO substrates. The ∼1550 cm^{-1} C−C stretching peak associated with the presence of TMPyP can be identified for concentrations as low as 10^{-5} M on CNF and 10^{-3} M on GO (Figure 5d,e). The dependence of the coverage of the porphyrin adlayer on the concentration of the solution used is outlined in Table S1, showing that the limit of detection for CNF is reached when more than 10 monolayers of TMPyP are present on the cellulose surface. As we have previously shown in a computational study, TMPyP grows in a disordered way, beyond a single molecule growth, resulting in a generation of 3D clusters.[61] The data suggests that only when

https://doi.org/10.1021/acssuschemeng.1c06685
ACS Sustainable Chem. Eng. 2021, 9, 16808−16819

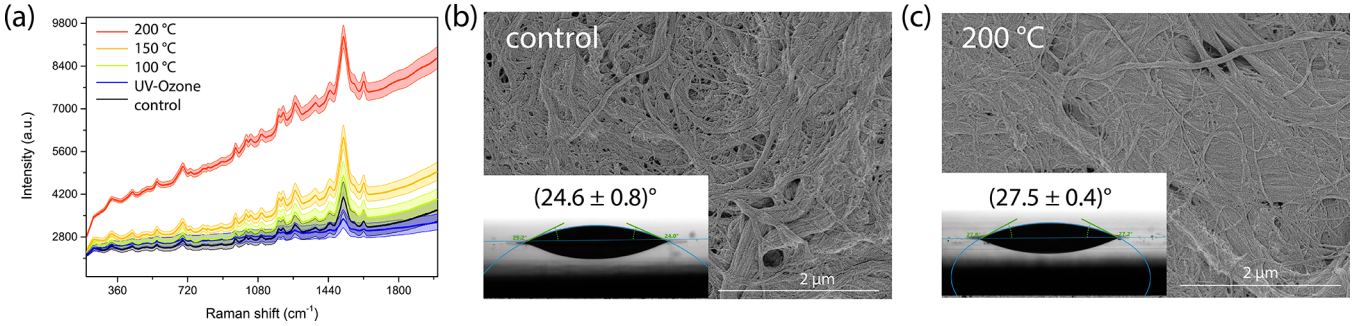

Figure 6. (a) Normalized SERS spectra of 10^{-4} M TMPyP on pristine and heat-treated CNF substrate. (b, c) SEM images of CNF untreated and annealed at 200 °C along with the contact angle measurements for the two surfaces.

several layers of porphyrins are present in the sample and clustering takes place, the molecule can be detected.

Although the spectra of TMPyP on CNF and AgNPs were comparable in terms of intensity, the detection limit on silver is much lower, with 10^{-7} M TMPyP still being detectable (Figure S15), showing the main limitation of this approach. Metal-free substrates are however known to be characterized by lower detection limits, rarely reaching values as low as 10^{-6} and 10^{-7} M, associated with less than one monolayer coverage of the molecules on the substrate.[49] The spectrum of 10^{-5} M TMPyP on CNF is however clear and several clear peaks associated with the presence of the analyte can be distinguished in the spectrum, as highlighted in Figure 5f, making the cellulose-based substrates a promising platform for metal-free low-concentration molecule detection.

Finally, we investigated the effect of employing heat treatment of the CNF substrate on its performance as a SERS platform for the detection of porphyrins. Substrate annealing in air has been shown to be a simple and effective way of improving the SERS performance due to effects associated with oxygen defect introduction and the change of wettability on the substrate.[67] Figure 6a demonstrates that following heat annealing of the CNF substrate for 40 min at 200 °C, the intensity of both the overall TMPyP signal and the relative peak strength can be further enhanced 2-fold. The effect can be attributed to the increase in the hydrophobicity of the substrate after treatment, resulting in the reduction of spreading of the solution drop after deposition, and therefore an artificial increase in the analyte molecule concentration.[11] The contact angle for a water droplet on the untreated substrate was measured to be 24.6 ± 0.8°, which then increases to 27.5 ± 0.4° following treatment. Figure 6b,c shows SEM images of the CNF substrate prior to and following treatment, demonstrating that the sample is stable at high temperatures and that no significant changes in the sample topography can be observed. The stability of the samples was also investigated using EDX, as outlined in Figure S18 and Table S3. The composition of the samples remains mostly unchanged, with the amount of oxygen increasing slightly following the annealing in an oxygen-rich atmosphere, suggesting oxidation of the sample, which has previously been shown for inorganic semiconductors.[68] Although any drying effects associated with the heat treatments are temporary, as water may be adsorbed on the cellulose surface from the atmosphere, the changes in the contact angle values and the associated SERS signal enhancement on treated samples are preserved for several days following treatment.

CONCLUSIONS

We have demonstrated that randomly distributed cellulose nanofibers are an efficient metal-free SERS platform that can be used for the detection of porphyrin-like molecules. We show that the SERS enhancement observed varies between molecules with different ligands with the highest 96-fold relative peak enhancement being observed for cationic and water-soluble TMPyP. We propose that the observed enhancement is a combination of multiple processes occurring with a charge transfer mechanism increasing the rate of inelastically scattered light taking place for all of the porphyrin molecules studied. The notably high enhancement of TMPyP could be explained by additional processes associated with the counterions in the porphyrin species interacting with the −OH groups of cellulose, resulting in the generation of a dipole moment and an electric field in the porphyrin adlayer, which is further confirmed by the reduction of the Raman signal when cellulose derivative materials are used as a substrate. We demonstrated that the Raman peak positions shift for the TMPyP adsorbed on cellulose, which suggests a possible change in the crystal structure of the porphyrin adlayer and the disruption in the nanorod self-assembly process of the molecules. TMPyP was shown to self-assemble into ordered nanorod-like structures on silicon substrates, while forming disordered 3D clusters on cellulose, as supported by confocal fluorescence images and previously published computational data. Due to the fact that similar SERS enhancements can be obtained for different types of cellulose derivative-based substrates, we propose that the interaction between the cellulose backbone and the tetrapyrrole ring of the porphyrin could be responsible for the change in the porphyrin adsorption properties. The detection limit for TMPyP on CNF is 10^{-5} M, and the substrate efficiency can be further enhanced 2-fold by employing a heat treatment process. The CNF platform is comparable to other plasmon-free SERS substrates such as graphene, making the approach viable for substrate design in the fields of medicine, security, and environmental science.

EXPERIMENTAL SECTION

Sample Preparation. Sigma Aldrich provided all of the chemicals unless stated otherwise. All chemicals were used directly without any further purification.

Cellulose nanofibers (CNF; prepared by supermass colloider; 30−80 nm width, >100 μm length, 3 wt % in water) and TEMPO-oxidized cellulose nanofibers (TEMPO-CNF; 50 nm width, 0.5−80 μm, 1 wt % in water) were provided by Cellulose Lab. For concentration studies, CNF and TEMPO-CNF were diluted in distilled water down to the desired concentration and then sonicated

https://doi.org/10.1021/acssuschemeng.1c06685
ACS Sustainable Chem. Eng. 2021, 9, 16808−16819

for 20 min using a Fisherbrand FB15046 Ultrasonic Cleaning Bath to ensure a uniform distribution of the fibers.

Cellulose acetate powder (CA; average M_n ~30 000 by gel permeation chromatography (GPC); CAS Number: 9004-35-7) was dissolved in acetone at 1 wt % and stirred overnight. Hydroxypropyl cellulose powder (HPC; average M_w ~100 000; CAS: 9004-64-2) was dissolved in deionized water at 1 wt %. The substrates were then prepared by drop-casting the cellulose (CNF, TEMPO-CNF, CA, or HPC) on silicon substrate and left to dry. For the heat treatment experiment, the CNF samples were annealed at different temperatures in an oven (Genlab Limited) for 40 min.

Graphene oxide (GO; product code 763705; 2 mg/mL dispersion in H_2O) was diluted in distilled water down to 0.2 mg/mL and then deposited on a silicon substrate. Silver nanoparticles (AgNPs; product code 730807; 40 nm particle size, 0.02 mg/mL in aqueous buffer, contains sodium citrate as a stabilizer) were also used without any subsequent dilution.

Preparation of Probe Molecule Solutions. Powders of meso-tetraphenylporphyrin (TPP; CAS Number 917-23-7), meso-tetra(*N*-methyl-4-pyridyl)porphine tetrachloride (TMPyP; T40125, Frontier Scientific), meso-tetra(*N*-methyl-4-pyridyl)porphine tetratosylate salt (TMPyP; CAS Number 36951-72-1), 5,10,15,20-tetrakis(4-trimethylammoniophenyl)porphyrin tetra(*p*-toluenesulfonate) (TMAP, CAS: 69458-20-4), meso-tetra(4-sulfonatophenyl)porphine tetrasodium salt dodecahydrate (TPPS; T40699, Frontier Scientific), and meso-tetra(4-carboxyphenyl)porphine (TCPP; T790, Frontier Scientific) were used. Additionally, the following nonporphyrin molecules were used as analytes: methyl green (zinc chloride salt, ~85%; CAS: 7114-03-6), victoria blue B (VBB; CAS: 2580-56-5), and methyl violet 2B (MV2B; CAS: 8004-87-3).

Water-soluble porphyrin solutions (TMPyP, TPPS, TMAP, and TCPP) as well as MG, VBB, and MV2B were prepared by dissolving the powders in distilled water at an initial concentration of 10^{-2} or 10^{-3} M. TPP solution was prepared in dichloromethane (CH_2Cl_2, CAS Number: 75-09-2). All of the probe molecule solutions used were diluted down to a concentration of 10^{-4} M using the solvent they were initially dissolved in. Crystal violet 1% aqueous solution (CAS Number: 548-62-9) was diluted in distilled water down to the concentration of 10^{-4} M. The solubility of the molecules was assessed visually at room temperature. All of the molecules dissolved in distilled water/CH_2Cl_2 at a concentration of 10^{-3} M resulted in an optically clear solution with no visible aggregates.

Raman Spectroscopy. The measurement was performed using a bespoke Raman system consisting of a monochromatic laser (HeNe, ThorLabs) with a beam splitter and a long-pass filter (RazorEdge, Semrock), an inverted optical microscope (IX71, Olympus), a spectrograph (SP-2300i, Princeton Instruments), and a CCD camera (iDus 401, Andor).[69−72] A 50× objective was used to focus the laser (532 nm wavelength, 5 mW incident power regulated by an attenuator) and collect the Raman signal with an exposure time of 2 s in an accumulation mode (10 accumulations). The CCD camera was calibrated over the spectral window using the Raman spectrum of toluene. To take spatial variability into consideration, an average signal from 10 different spots on the sample was reported.

UV−Vis Absorption Spectroscopy. Optical absorbance measurements were performed using an absorbance spectrometer (V-650, JASCO, Inc.) under the following settings: 1 nm step size, 1 nm bandwidth, and 400 nm/min scan speed across a 190−900 nm range. The measurements were performed for samples deposited on a coverslip or as a solution in a quartz cuvette.

Fourier Transform Infrared Spectroscopy. Fourier transform infrared (FTIR) spectra were collected using an α Platinum Bruker system. To record FTIR spectra, the substrates on a coverslip or in solution were placed onto the ATR interface. Spectra were collected using transmission mode scanning in the range of 400−4000 cm^{-1}.

Scanning Electron Microscopy. High-resolution scanning electron microscopy (SEM) images were obtained using a Regulus8230 Scanning Electron Microscopy employed with an energy-dispersive X-ray spectroscopy (EDX) system following the coating of the substrates with a 5 nm thick layer of iridium.

Atomic Force Microscopy. AFM images were obtained using an MFP-3D Asylum Research instrument operating in tapping mode. Monolithic silicon Tap300Al-G probes with Aluminum Reflective Coating (BudgetSensors) were used to obtain the images. The tips used were characterized by the following specifications: 40 N/m (20−75 N/m) force constant, 300 kHz (200−400 kHz) resonance frequency, 125 μm (115−135 μm) length. The surface area was calculated using Gwyddion software based on a 20 μm height image of the sample.

Fluorescence Confocal Microscopy. Fluorescence confocal microscopy images were obtained using the Leica TCS SP8 confocal system using a white light laser set to 532 nm, and internal HyD GaAsP SMD detector. A 63× oil objective was used and the samples were imaged through a coverslip in air, without the introduction of a mounting medium.

Contact Angle. A contact angle measuring system (Kruss Advance Drop Shape Analyser DSA25E) was used to measure contact angles of droplets of deionized water (Milli-Q) on treated and untreated substrates.

■ ASSOCIATED CONTENT

Supporting Information

The Supporting Information is available free of charge at https://pubs.acs.org/doi/10.1021/acssuschemeng.1c06685.

Dependence of the porphyrin overlayer coverage on the concentration of the analyte molecule used (Table S1); calculated SERS signal enhancements (Table S2); composition of the pristine and treated CNF samples (Table S3); method of calculation of the overall Raman peak intensity and the relative background-subtracted peak intensity from the spectrum (Figure S1); SERS spectra on different types of supporting subsrtates (Figure S2); SERS spectra from 30 randomly selected spots on the CNF sample (Figure S3); SERS spectra of the nonporphyrin molecules on CNF (Figure S4); band diagram showing possible charge transfer between the CNF substrate and the nonporphyrin molecules (Figure S5); normalized SERS spectra of porphyrins (Figure S6); fluorescence confocal microscopy images of porphyrins (Figure S7); SEM images of porphyrins (Figure S8); SERS spectra of TMPyP with different counterions (Figure S9); band diagram showing possible charge transfer between the CNF substrate and the porphyrin molecules (Figure S10); chemical structure of the cellulose derivative molecules (Figure S11); AFM images of different subsrtates (Figure S12); SERS spectra used for calculation of enhancement (Figure S13); contact angle measurements (Figure S14); normalized SERS spectra used for calculation of the detection limit (Figure S15); normalized Raman spectra following CNF dillution (Figure S16); SEM images (Figure S17); and electron microscopy image and energy-dispersive X-ray spectroscopy mapping of CNF (Figure S18) (PDF)

■ AUTHOR INFORMATION

Corresponding Author

James H. Rice − *School of Physics, University College Dublin, Dublin 4, Ireland;* orcid.org/0000-0002-1035-5708; Email: james.rice@ucd.ie

Authors

Agata Fularz − *School of Physics, University College Dublin, Dublin 4, Ireland;* orcid.org/0000-0001-7794-6177

Sawsan Almohammed − *School of Physics, University College Dublin, Dublin 4, Ireland; Conway Institute of Biomolecular and Biomedical Research, University College Dublin, Dublin 4, Ireland;* orcid.org/0000-0002-5990-5088

Complete contact information is available at: https://pubs.acs.org/10.1021/acssuschemeng.1c06685

Author Contributions

A.F., S.A., and J.H.R. designed the experiments and developed the experimental setup. A.F. and S.A. performed UV−vis measurements. A.F. carried out sample preparation and Raman, FTIR, SEM, AFM, and confocal fluorescence microscopy measurements. All authors analyzed data, discussed results, and wrote and reviewed the manuscript.

Funding

This publication has emanated from research conducted with the financial support of the UCD School of Physics (SIRAT—Scholarship in Research and Teaching). The work was supported by Sustainable Energy Authority of Ireland (SEAI).

Notes

The authors declare no competing financial interest.

■ ACKNOWLEDGMENTS

The authors thank Ian Reid for access to SEM; Gareth Redmond for access to UV−vis spectroscopy; Aaron Martin and Hans Eckhardt for access to FTIR spectroscopy; and Brian Rodriguez for access to AFM, the oven, and UV-Ozone. The authors also thank Una Prendergast for assistance with confocal microscopy, as well as Dennis Dowling and Frank Vaughan for contact angle measurements. They thank Pietro Ballone for the insightful comments and discussions.

■ REFERENCES

(1) Downes, A.; Elfick, A. Raman Spectroscopy and Related Techniques in Biomedicine. *Sensors* **2010**, *10*, 1871−1889.
(2) Halvorson, R. A.; Vikesland, P. J. Surface-Enhanced Raman Spectroscopy (SERS) for Environmental Analyses. *Environ. Sci. Technol.* **2010**, *44*, 7749−7755.
(3) Muehlethaler, C.; Leona, M.; Lombardi, J. R. Review of Surface Enhanced Raman Scattering Applications in Forensic Science. *Anal. Chem.* **2016**, *88*, 152−169.
(4) Demirel, G.; Usta, H.; Yilmaz, M.; Celik, M.; Alidagi, H. A.; Buyukserin, F. Surface-Enhanced Raman Spectroscopy (SERS): An Adventure from Plasmonic Metals to Organic Semiconductors as SERS Platforms. *J. Mater. Chem. C* **2018**, *6*, 5314−5335.
(5) Mosier-Boss, P. Review of SERS Substrates for Chemical Sensing. *Nanomaterials* **2017**, *7*, No. 142.
(6) Bantz, K. C.; Meyer, A. F.; Wittenberg, N. J.; Im, H.; Kurtuluş, Ö.; Lee, S. H.; Lindquist, N. C.; Oh, S. H.; Haynes, C. L. Recent Progress in SERS Biosensing. *Phys. Chem. Chem. Phys.* **2011**, *13*, 11551−11567.
(7) Ding, S.-Y.; You, E.-M.; Tian, Z.-Q.; Moskovits, M. Electromagnetic Theories of Surface-Enhanced Raman Spectroscopy. *Chem. Soc. Rev.* **2017**, *46*, 4042−4076.
(8) Fateixa, S.; Nogueira, H. I. S.; Trindade, T. Hybrid Nanostructures for SERS: Materials Development and Chemical Detection. *Phys. Chem. Chem. Phys.* **2015**, *17*, 21046−21071.
(9) Stiles, P. L.; Dieringer, J. A.; Shah, N. C.; Van Duyne, R. P. Surface-Enhanced Raman Spectroscopy. *Annu. Rev. Anal. Chem.* **2008**, *1*, 601−626.
(10) Lan, L.; Gao, Y.; Fan, X.; Li, M.; Hao, Q.; Qiu, T. The Origin of Ultrasensitive SERS Sensing beyond Plasmonics. *Front. Phys.* **2021**, No. 43300.
(11) Yilmaz, M.; Babur, E.; Ozdemir, M.; Gieseking, R. L.; Dede, Y.; Tamer, U.; Schatz, G. C.; Facchetti, A.; Usta, H.; Demirel, G. Nanostructured Organic Semiconductor Films for Molecular Detection with Surface-Enhanced Raman Spectroscopy. *Nat. Mater.* **2017**, *16*, 918−924.
(12) O'Sullvian, A. C. Cellulose: The Structure Slowly Unravels. *Cellulose* **1997**, *4*, 173−207.
(13) Xiong, Z.; Lin, M.; Lin, H.; Huang, M. Facile Synthesis of Cellulose Nanofiber Nanocomposite as a SERS Substrate for Detection of Thiram in Juice. *Carbohydr. Polym.* **2018**, *189*, 79−86.
(14) Song, Y.; Shi, Z.; Hu, G. H.; Xiong, C.; Isogai, A.; Yang, Q. Recent Advances in Cellulose-Based Piezoelectric and Triboelectric Nanogenerators for Energy Harvesting: A Review. *J. Mater. Chem. A* **2021**, *9*, 1910−1937.
(15) Simão, C. D.; Reparaz, J. S.; Wagner, M. R.; Graczykowski, B.; Kreuzer, M.; Ruiz-Blanco, Y. B.; García, Y.; Malho, J. M.; Goñi, A. R.; Ahopelto, J.; Sotomayor Torres, C. M. Optical and Mechanical Properties of Nanofibrillated Cellulose: Toward a Robust Platform for next-Generation Green Technologies. *Carbohydr. Polym.* **2015**, *126*, 40−46.
(16) Espinha, A.; Dore, C.; Matricardi, C.; Alonso, M. I.; Goñi, A. R.; Mihi, A. Hydroxypropyl Cellulose Photonic Architectures by Soft Nanoimprinting Lithography. *Nat. Photonics* **2018**, *12*, 343−348.
(17) Liou, P.; Nayigiziki, F. X.; Kong, F.; Mustapha, A.; Lin, M. Cellulose Nanofibers Coated with Silver Nanoparticles as a SERS Platform for Detection of Pesticides in Apples. *Carbohydr. Polym.* **2017**, *157*, 643−650.
(18) Kim, D.; Ko, Y.; Kwon, G.; Kim, U. J.; Lee, J. H.; You, J. 2,2,6,6-Tetramethylpiperidine-1-Oxy-Oxidized Cellulose Nanofiber-Based Nanocomposite Papers for Facile in Situ Surface-Enhanced Raman Scattering Detection. *ACS Sustainable Chem. Eng.* **2019**, *7*, 15640−15647.
(19) Van Rie, J.; Thielemans, W. Cellulose-Gold Nanoparticle Hybrid Materials. *Nanoscale* **2017**, *9*, 8525−8554.
(20) Lu, Y.; Luo, Y.; Lin, Z.; Huang, J. A Silver-Nanoparticle/Cellulose-Nanofiber Composite as a Highly Effective Substrate for Surface-Enhanced Raman Spectroscopy. *Beilstein J. Nanotechnol.* **2019**, *10*, 1270−1279.
(21) Rusin, C. J.; El Bakkari, M.; Du, R.; Boluk, Y.; McDermott, M. T. Plasmonic Cellulose Nanofibers as Water-Dispersible Surface-Enhanced Raman Scattering Substrates. *ACS Appl. Nano Mater.* **2020**, *3*, 6584−6597.
(22) Caligiuri, V.; Tedeschi, G.; Palei, M.; Miscuglio, M.; Martin-Garcia, B.; Guzman-Puyol, S.; Hedayati, M. K.; Kristensen, A.; Athanassiou, A.; Cingolani, R.; Sorger, V. J.; Salerno, M.; Bonaccorso, F.; Krahne, R.; Heredia-Guerrero, J. A. Biodegradable and Insoluble Cellulose Photonic Crystals and Metasurfaces. *ACS Nano* **2020**, *14*, 9502−9511.
(23) Yan, D.; Qiu, L.; Xue, M.; Meng, Z.; Wang, Y. A Flexible Surface-Enhanced Raman Substrates Based on Cellulose Photonic Crystal/Ag-Nanoparticles Composite. *Mater. Des.* **2019**, *165*, No. 107601.
(24) Marques, H. M.; Brown, K. L. Molecular Mechanics and Molecular Dynamics Simulations of Porphyrins, Metalloporphyrins, Heme Proteins and Cobalt Corrinoids. *Coord. Chem. Rev.* **2002**, *225*, 123−158.
(25) Collman, J. P.; Fu, L. Synthetic Models for Hemoglobin and Myoglobin. *Acc. Chem. Res.* **1999**, *32*, 455−463.
(26) Perutz, M. F.; Fermi, G.; Luisi, B.; et al. Stereochemistry of Cooperative Mechanisms in Hemoglobin. *Acc. Chem. Res.* **1987**, *20*, 309−321.
(27) Alberta, J. A.; Andersson, L. A.; Dawson, J. H. Spectroscopic Characterization of Secondary Amine Mono-Oxygenase. Comparison to Cytochrome P-450 and Myoglobin. *J. Biol. Chem.* **1989**, *264*, 20467−20473.
(28) Drain, C. M.; Varotto, A.; Radivojevic, I. Self-Organized Porphyrinic Materials. *Chem. Rev.* **2009**, *109*, 1630−1658.
(29) Huang, X.; Groves, J. T. Oxygen Activation and Radical Transformations in Heme Proteins and Metalloporphyrins. *Chem. Rev.* **2018**, *118*, 2491−2553.

(30) English, A. M.; Tsaprailis, G. Catalytic Structure−Function Relationships in Heme Peroxidases. *Adv. Inorg. Chem.* **1995**, *43*, 79−125.
(31) Larue, L.; Ben Mihoub, A.; Youssef, Z.; Colombeau, L.; Acherar, S.; André, J. C.; Arnoux, P.; Baros, F.; Vermandel, M.; Frochot, C. Using X-Rays in Photodynamic Therapy: An Overview. *Photochem. Photobiol. Sci.* **2018**, *17*, 1612−1650.
(32) Nakagaki, S.; Castro, K. A. D. F.; Neves, M.; da, G. P. M. S.; do Amparo Faustino, M.; Iamamoto, Y. The Research on Porphyrins and Analogues in Brazil: A Small Review Covering Catalytic and Other Applications since the Beginning at Universidade de São Paulo in Ribeirão Preto until the Joint Venture between Brazilian Researchers and Colleagues from Universidade de Aveiro, Portugal. *J. Braz. Chem. Soc.* **2019**, *30*, 2501−2535.
(33) Usmani, M. A.; Khan, I.; Gazal, U.; Mohamad Haafiz, M. K.; Bhatk, A. H. Interplay of Polymer Bionanocomposites and Significance of Ionic Liquids for Heavy Metal Removal. In *Polymer-Based Nanocomposites for Energy and Environmental Applications*; Woodhead Publishing Series in Composites Science and Engineering; Elsevier Ltd., 2018; pp 441−463.
(34) Vipin, A. K.; Fugetsu, B.; Sakata, I.; Isogai, A.; Endo, M.; Li, M.; Dresselhaus, M. S. Cellulose Nanofiber Backboned Prussian Blue Nanoparticles as Powerful Adsorbents for the Selective Elimination of Radioactive Cesium. *Sci. Rep.* **2016**, *6*, No. 37009.
(35) Hai, T. A. P.; Sugimoto, R. Surface Functionalization of Cellulose with Poly(3-Hexylthiophene) via Novel Oxidative Polymerization. *Carbohydr. Polym.* **2018**, *179*, 221−227.
(36) Fularz, A.; Almohammed, S.; Rice, J. H. Electric Field-Induced Boron Nitride/Silver Nanoparticle Template Discharge for Fluorescence Signal Enhancement. *J. Appl. Phys.* **2020**, *128*, No. 213105.
(37) Khairutdinov, R. F.; Serpone, N. Photoluminescence and Transient Spectroscopy of Free Base Porphyrin Aggregates. *J. Phys. Chem. B* **1999**, *103*, 761−769.
(38) Harsha Vardhan Reddy, M.; Al-Shammari, R. M.; Al-Attar, N.; Kennedy, E.; Rogers, L.; Lopez, S.; Senge, M. O.; Keyes, T. E.; Rice, J. H. Micro- or Nanorod and Nanosphere Structures Derived from a Series of Phenyl-Porphyrins. *Phys. Chem. Chem. Phys.* **2014**, *16*, 4386−4393.
(39) Wang, R. X.; Fan, J. J.; Fan, Y. J.; Zhong, J. P.; Wang, L.; Sun, S. G.; Shen, X. C. Platinum Nanoparticles on Porphyrin Functionalized Graphene Nanosheets as a Superior Catalyst for Methanol Electrooxidation. *Nanoscale* **2014**, *6*, 14999−15007.
(40) Jhonsi, M. A.; Renganathan, R. Photoinduced Electron Transfer from Meso- Tetrakis (N-Methylpyridyl) Porphyrin (TMPyP) to Colloidal CdS. *Z. Phys. Chem.* **2008**, *222*, 1601−1610.
(41) Chen, W.; He, H.; Zhu, H.; Cheng, M.; Li, Y.; Wang, S. Thermo-Responsive Cellulose-Based Material with Switchable Wettability for Controllable Oil/Water Separation. *Polymers* **2018**, *10*, No. 592.
(42) Atykyan, N.; Revin, V.; Shutova, V. Raman and FT-IR Spectroscopy Investigation the Cellulose Structural Differences from Bacteria Gluconacetobacter Sucrofermentans during the Different Regimes of Cultivation on a Molasses Media. *AMB Express* **2020**, *10*, No. 84.
(43) Mojet, B. L.; Ebbesen, S. D.; Lefferts, L. Light at the Interface: The Potential of Attenuated Total Reflection Infrared Spectroscopy for Understanding Heterogeneous Catalysis in Water. *Chem. Soc. Rev.* **2010**, *39*, 4643−4655.
(44) Fu, H.; Bao, H.; Zhang, H.; Zhao, Q.; Zhou, L.; Zhu, S.; Wei, Y.; Li, Y.; Cai, W. Quantitative Surface-Enhanced Raman Spectroscopy for Field Detections Based on Structurally Homogeneous Silver-Coated Silicon Nanocone Arrays. *ACS Omega* **2021**, *6*, 18928−18938.
(45) Almohammed, S.; Zhang, F.; Rodriguez, B. J.; Rice, J. H. Electric Field-Induced Chemical Surface-Enhanced Raman Spectroscopy Enhancement from Aligned Peptide Nanotube-Graphene Oxide Templates for Universal Trace Detection of Biomolecules. *J. Phys. Chem. Lett.* **2019**, *10*, 1878−1887.
(46) Silver, A.; Kitadai, H.; Liu, H.; Granzier-Nakajima, T.; Terrones, M.; Ling, X.; Huang, S. Chemical and Bio Sensing Using Graphene-Enhanced Raman Spectroscopy. *Nanomaterials* **2019**, *9*, No. 516.
(47) Xu, W.; Ling, X.; Xiao, J.; Dresselhaus, M. S.; Kong, J.; Xu, H.; Liu, Z.; Zhang, J. Surface Enhanced Raman Spectroscopy on a Flat Graphene Surface. *Proc. Natl. Acad. Sci. U.S.A.* **2012**, *109*, 9281−9286.
(48) Xu, W.; Mao, N.; Zhang, J. Graphene: A Platform for Surface-Enhanced Raman Spectroscopy. *Small* **2013**, *9*, 1206−1224.
(49) Tan, X.; Melkersson, J.; Wu, S.; Wang, L.; Zhang, J. Noble-Metal-Free Materials for Surface-Enhanced Raman Spectroscopy Detection. *ChemPhysChem* **2016**, 2630−2639.
(50) Itabashi, M.; Masuda, T.; Itoh, K. Surface-Enhanced Resonance Raman Scattering Study Of The Reduction Processes Of Meso-Tetrakis(4-N-Methylpyridyl)Porphine Adsorbed At Silver Electrode Surfaces. *J. Electroanal. Chem. Interfacial Electrochem.* **1984**, *165*, 265−278.
(51) Šubr, M.; Petr, M.; Peksa, V.; Kylián, O.; Hanuš, J.; Procházka, M. Ag Nanorod Arrays for SERS: Aspects of Spectral Reproducibility, Surface Contamination, and Spectral Sensitivity. *J. Nanomater.* **2015**, *2015*, 1−7.
(52) Qu, J.; Arnold, D. P.; Fredericks, P. M. Concentration Dependence of the SERS of Some Water-Soluble-Cationic Porphyrins on an Electrochemically Prepared Silver Surface. *J. Raman Spectrosc.* **2000**, *31*, 469−473.
(53) Aydin, M. DFT and Raman Spectroscopy of Porphyrin Derivatives: Tetraphenylporphine (TPP). *Vib. Spectrosc.* **2013**, *68*, 141−152.
(54) Zhang, Y. H.; Chen, D. M.; He, T.; Liu, F. C. Raman and Infrared Spectral Study of Meso-Sulfonatophenyl Substituted Porphyrins (TPPSn, n = 1, 2A, 2O, 3, 4). *Spectrochim. Acta, Part A* **2003**, *59*, 87−101.
(55) Wan, J.; Wang, H.; Wu, Z.; Shun, Y. C.; Zheng, X.; Phillips, D. L. Resonance Raman Spectroscopy and Density Functional Theory Calculation Study of Photodecay Dynamics of Tetra(4-Carboxyphenyl) Porphyrin. *Phys. Chem. Chem. Phys.* **2011**, *13*, 10183−10190.
(56) Muresan, A. Z.; Lindsey, J. S. Design and Synthesis of Water-Soluble Bioconjugatable Trans-AB-Porphyrins. *Tetrahedron* **2008**, *64*, 11440−11448.
(57) Wu, J. B.; Lin, M. L.; Cong, X.; Liu, H. N.; Tan, P. H. Raman Spectroscopy of Graphene-Based Materials and Its Applications in Related Devices. *Chem. Soc. Rev.* **2018**, *47*, 1822−1873.
(58) Medforth, C. J.; Wang, Z.; Martin, K. E.; Song, Y.; Jacobsen, J. L.; Shelnutt, J. A. Self-Assembled Porphyrin Nanostructures. *Chem. Commun.* **2009**, 7261−7277.
(59) Hamor, M. J.; Hamor, T. A.; Hoard, J. L. The Structure of Crystalline Tetraphenylporphine. The Stereochemical Nature of the Porphine Skeleton. *J. Am. Chem. Soc.* **1964**, *86*, 1938−1942.
(60) Silvers, S. J.; Tulinsky, A. The Crystal and Molecular Structure of Triclinic Tetraphenylporphyrin. *J. Am. Chem. Soc.* **1967**, *89*, 3331−3337.
(61) Fularz, A.; Rice, J. H.; Ballone, P. Morphology of Nanometric Overlayers Made of Porphyrin-Type Molecules Physisorbed on the Surface of Cellulose Iβ Crystals and and Nanocrystals. *J. Phys. Chem. B* **2021**, 11432−11443.
(62) Campione, M.; Hogan, C.; Palummo, M.; Bossi, A.; Yivlialin, R.; Bussetti, G. Close-Packed Arrangements of Flat-On Free-Base Porphyrins Driven by van Der Waals Epitaxy. *Cryst. Growth Des.* **2020**, *20*, 7450−7459.
(63) Djuric, T.; Ules, T.; Gusenleitner, S.; Kayunkid, N.; Plank, H.; Hlawacek, G.; Teichert, C.; Brinkmann, M.; Ramsey, M.; Resel, R. Substrate Selected Polymorphism of Epitaxially Aligned Tetraphenyl-Porphyrin Thin Films. *Phys. Chem. Chem. Phys.* **2012**, *14*, 262−272.
(64) Kuzmin, S. M.; Chulovskaya, S. A.; Parfenyuk, V. I. Structures and Properties of Porphyrin-Based Film Materials Part I. The Films Obtained via Vapor-Assisted Methods. *Adv. Colloid Interface Sci.* **2018**, *253*, 23−34.
(65) Pérez-Morales, M.; De Miguel, G.; Bolink, H. J.; Martín-Romero, M. T.; Camacho, L. Soret Emission from Water-Soluble Porphyrin Thin Films: Effect on the Electroluminescence Response. *J. Mater. Chem.* **2009**, *19*, 4255−4260.

https://doi.org/10.1021/acssuschemeng.1c06685
ACS Sustainable Chem. Eng. 2021, 9, 16808−16819

(66) Srivastava, D.; Kuklin, M. S.; Ahopelto, J.; Karttunen, A. J. Electronic Band Structures of Pristine and Chemically Modified Cellulose Allomorphs. *Carbohydr. Polym.* **2020**, *243*, No. 116440.
(67) Fularz, A.; Almohammed, S.; Rice, J. H. Oxygen Incorporation-Induced SERS Enhancement in Silver Nanoparticle-Decorated ZnO Nanowires. *ACS Appl. Nano Mater.* **2020**, *3*, 1666−1673.
(68) Rice, J. H.; Fularz, A.; Almohammed, S. Controlling Plasmon-Induced Photocatalytic Redox Reactions on WO3 Nanowire/AgNPs Substrates via Defect Engineering. *J. Phys. Chem. C* **2020**, *124*, 25351−25360.
(69) Almohammed, S.; Oladapo, S. O.; Ryan, K.; Kholkin, A. L.; Rice, J. H.; Rodriguez, B. J. Wettability Gradient-Induced Alignment of Peptide Nanotubes as Templates for Biosensing Applications. *RSC Adv.* **2016**, *6*, 41809−41815.
(70) Damm, S.; Craig Carville, N.; Manzo, M.; Gallo, K.; Lopez, S. G.; Keyes, T. E.; Forster, R. J.; Rodriguez, B. J.; Rice, J. H. Surface Enhanced Luminescence and Raman Scattering from Ferroelectrically Defined Ag Nanopatterned Arrays. *Appl. Phys. Lett.* **2013**, *103*, No. 083105.
(71) Damm, S.; Fedele, S.; Murphy, A.; Holsgrove, K.; Arredondo, M.; Pollard, R.; Barry, J. N.; Dowling, D. P.; Rice, J. H. Plasmon Enhanced Fluorescence Studies from Aligned Gold Nanorod Arrays Modified with SiO2 Spacer Layers. *Appl. Phys. Lett.* **2015**, *106*, No. 183109.
(72) Almohammed, S.; Fedele, S.; Rodriguez, B. J.; Rice, J. H. Aligned Diphenylalanine Nanotube−Silver Nanoparticle Templates for High-Sensitivity Surface-Enhanced Raman Scattering. *J. Raman Spectrosc.* **2017**, *48*, 1799−1807.

https://doi.org/10.1021/acssuschemeng.1c06685
ACS Sustainable Chem. Eng. 2021, 9, 16808−16819